HEFAT2010
7th International Conference on Heat Transfer, Fluid Mechanics and Thermodynamics
19-21 July 2010
Antalya, Turkey

EXPERIMENTAL INVESTIGATION OF THE REDUCED FREQUENCY EFFECTS ON A PLUNGING AIRFOIL NEAR STATIC STALL REGION

F. Ajalli*, M. Mani, M. Saeedi
Department of Aerospace Engineering,
AmirKabir University of Technology, Tehran, Iran
M.R. Soltani
Department of Aerospace Engineering,
Sharif University of Technology, Tehran, Iran
E-mail: fajalli59@gmail.com

ABSTRACT

Details of pressure distributions and aerodynamic coefficients on a two dimensional plunging airfoil, at low speed wind tunnel are presented. Dynamic motion was produced by plunging the model over a range of reduced frequencies, and mean angles of attack. The Reynolds number in the present test was held fixed ($Re=1.5\times10^5$), and the reduced frequency was varied in almost wide range. During the oscillating motion, surface static pressure distribution was measured on the upper and lower side of the model. The aerodynamic loads were calculated from the surface pressure measurements. The flow structure was studied in stall onset region. The hysteresis loops of pressure coefficient and aerodynamic loads showed that the reduced frequency had important effects on the unsteady behaviors of the flow. Near static stall angle of attack, an energetic vortex structure at the airfoil leading edge was formed. This dynamic vortex allowed the airfoil to achieve much higher lift coefficients before significant separation occurred.

INTRODUCTION

One of the basic problems of flight dynamics is the formulation of aerodynamic forces and moments acting on an aircraft in an arbitrary motion. For many years, the aerodynamic functions were approximated by linear expressions. With the increasing emphasis on high angle of attack flights, aerodynamic predictions technology has moved into the realm of dynamically separated flows and nonlinear responses, creating a new generation of experimental and analytical problems. The additions of nonlinear terms are very important and can not be omitted in the control field. These considerations were many times questioned based on the studies of unsteady aerodynamics [1, 2]. Helicopter Rotor blade sections encounter large time dependent variations in angle of attack that are a result of control input angles, blade flapping, structural response and wake inflow. In addition, the blade sections encounter substantial periodic variations in local velocity, Mach number and sweep angle.

NOMENCLATURE

c	[m]	airfoil chord
C_P	[-]	static pressure coefficient
f	[Hz]	frequency
k	[-]	reduce frequency, $\pi fc/V$
h	[cm]	plunging amplitude
$\dot{h}$	[m/s]	vertical velocity
α_{eq}	[deg]	equivalent angle of attack
α_{mean}	[deg]	mean incidence angle
C_l	[-]	lift coefficient
C_m	[-]	pitching moment coefficient about c/4
τ	[-]	non dimensional time, t/T
ω	[Hz]	angular velocity, $2\pi f$

Thus the unsteady aerodynamic behavior of the blade sections must be properly understood and carefully modeled to provide accurate predictions of the airloads and aeroelastic response of the rotor system. Dynamic stall is a problem of particular interest to the rotor analyst. This phenomenon occurs on the retreating blade of a helicopter rotor in high speed forward flight of during a maneuver. The importance of unsteady aerodynamics was considered by Harris and pruyen [3] when helicopter designers were unable to predict the performance of high speed helicopters using conventional aerodynamics. Ham and Garelick [4] observed the extra lift due to vortex formation

on the airfoil during the unsteady motion. Carta [5] was able to identify a pressure field on oscillating, two dimensional airfoils that was indicative of the passage of the vortex. Dynamic stall was then explored by McCroskey and fisher [6] on a model of a Helicopter rotor.

Many of the aerodynamic phenomena governing the behavior of wind turbine blades and helicopter rotors are known, but the details of the flow are still poorly understood and need to be predicted accurately. As a result of this inaccuracy, the actual loadings are under prediction [7]. Due to the complicated behaviours of unsteady forces during the plunging motion, numerical techniques are not able to predict accurately these variables yet, and relatively little experimental information is available about the precise fluid physics of oscillating airfoils. Also pure plunging airfoil motion has received relatively less attention than pitching motion. Therefore the main purpose of this experimental work is to study the pressure distributions at various locations of the Eppler-361 airfoil undergoing sinusoidal plunging oscillation at different reduced frequencies near static stall angle. This airfoil is vastly used for helicopter blades, wind turbine blades, etc. Fourteen pressure transducers and the on-line data acquisition system have significantly facilitated the study of the pressure distribution in the plunging airfoil. The surface pressure distribution have been integrated spatially to estimate the force and pitching moment time histories that correlate with the airfoil motion. These results can be used as a database for Computational Fluid Dynamic (CFD) code verifications too.

EXPERNAL FACILITY AND DATA PROCESSING

All experiments were performed in the subsonic wind tunnel of Amirkabir University of Technology. The wind tunnel is closed return type, and has a test section of approximately 45 cm in width, 45 cm in height, and 120cm in length. The Maximum flow speed in the test section of this tunnel is approximately 45m/s. The inlet of the tunnel has a 7.3:1 contraction ratio with four, anti-turbulence screens and honeycomb in settling chamber to reduce the tunnel turbulence to less than 0.1% at all speeds. The airfoil used in this study has an E-361 profile. A 15 cm constant chord airfoil model was designed and manufactured for the test program. The model was constructed to fully span the wind tunnel test section. Figure 1 shows the airfoil section along with the 14 pressure ports located on upper and lower surfaces used for static pressure measurements. The positions of the pressure ports on the suction surface were 5, 10, 15, 20, 30, 40, 50, 60, 70 and 80% chord and for pressure surface were 10, 20, 30, 70% chord locations.

Data was obtained by using differential pressure transducers with a quoted accuracy of 0.2% of full-scale pressure range. Due to the size of selected pressure transducers, the transducers could not be placed inside the model. Therefore, the connections between pressure ports and Pressure Transducers were made by tubes. Extensive experiments were conducted to ensure that the time taken for the pressure to reach the transducers is much less than the frequency response of the transducers themselves [8].

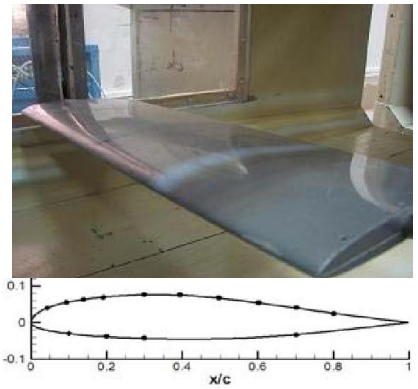

Figure 1 Airfoil section and location of pressure ports

To provide a stable pressure reference for the transducers, their "reference" tube were vented to the settling chamber of the wind tunnel. The data was processed by using analog to digital board. Oscillatory data was then digitally filtered using various cut-off and transition frequencies to find the best frequencies to fit the original data. The filtering process is necessary to eliminate the electrical noise from the genuine data. The driving mechanism of the plunging airfoil has a simple and versatile design which consists of motor, gears, cam, and shaft. The scotch-yoke configuration is used to create plunging motion. This mechanism can provide various frequencies (f), amplitudes (h) and mean angles of attack (α_{mean}). The motor and gear combination develop ranges of frequencies from 0.5 to 3Hz. The different amplitudes of oscillations (4, 6, 8 cm) are provided by using a cam system. Figure 2 shows the picture of oscillation mechanism. To take into account the inertial effects for the dynamic cases, the data collected in wind tunnel "off" position are subtracted from those collected during "on" position of the wind tunnel. Dynamic oscillatory data is an average of several cycles taken several times. The simultaneous position of the airfoil was measured using a potentiometer and the velocity feedback has been employed to minimize deviation in cycle to cycle motion fidelity. The sampling of each pressure channels was over 25 cycles of oscillatory motion and then ensemble averaged. The sampling rate was set 500 data points during the entire cycles. Based on the standard uncertainty, maximum variations from average pressure values did not exceeded 5% in the worst case.

Figure 2 Oscillation mechanism

RESULTS AND DISSCUSION

All experimental tests were conducted on a sinusoidal plunging airfoil at a free stream velocity of 15m/s, corresponding to Reynolds number of 1.5×10^5. The surface pressure distribution in dynamic motion was measured at mean angle of attack 10 degrees and different reduced frequencies for constant amplitude of oscillation h=8cm. The static pressures at angles of attack 0, 2, 5, 10, 12, 15, 17 and 20 degrees were measured too. The surface pressure distributions have been integrated spatially to estimate the force and pitching moment. The effects of the amplitudes of oscillations on the static pressure distribution in dynamic motion are presented in reference [9].

The time history of motion of the model was sorted as part of the data file. Figure 3 shows the sinusoidal variation of displacement with non-dimensional time. An "equivalent" angle of attack is usually defined for plunging motion [10,12], This equivalent angle of attack is mathematically defined as:

$$\alpha_{eq}(t)=\tan^{-1}\left(\frac{\dot{h}}{V}\right) \tag{1}$$

This for small angles can be identified to:

$$\alpha_{eq}(t)=\frac{\dot{h}}{V} \tag{2}$$

Substituting for $\dot{h}$ in terms of reduced frequency k, this gives:

$$\alpha_{eq}(t)=k\bar{h}\cos(\omega t) \tag{3}$$

Therefore, the "equivalent" angle of attack forcing amplitude for plunge can be derived written as:

$$\bar{\alpha}_{eq}=ik\bar{h} \tag{4}$$

Where $\bar{\alpha}_{eq}$ is in radians and $\bar{h}$ has been nondimensionalized with respect to semi-chord. Eq.4 is the transformation formula that relates displacement of a plunging motion to equivalent angle of attack. It is noticeable that the mean angle of attack should be added to the equivalent angle in Eq. 4. As shown in figures 3 and 4 the phase difference of displacement and equivalent angle of attack is 90 degrees. Figure 4 shows direct relation of the reduced frequency and equivalent angle of attack; it is obvious that increasing reduced frequency provides a wider range of angle of attack.

Figure 5 (a-h) shows the variations of the pressure coefficients against equivalent angle of attack at several positions, on both upper and lower surfaces at α_{mean}=10deg (near static stall angle) for several reduced frequencies. The model was set at an angle of attack 10 degrees and oscillated at different reduced frequencies. Note that the static stall angle for this airfoil occurred at 12degrees. The static data and direction of the variation of the equivalent angles of attack are shown too. It is to be noted that the direction of the motion to downward is assumed to be positive.

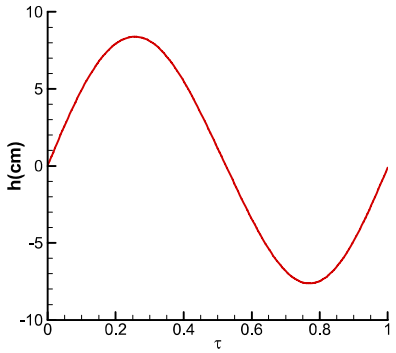

Figure 3 Sinusoidal variations of displacement (α_{mean}=10deg)

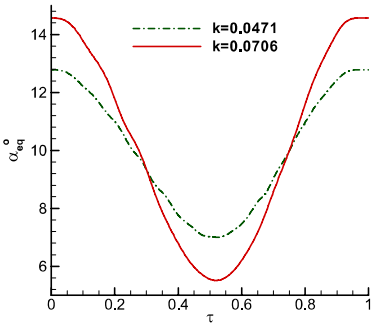

Figure 4 Variations of equivalent angle of attack vs. τ (α_{mean}=10deg)

The differences in values for the upstroke and down stroke motions create hysteresis loops where their shapes are functions of the mean angle of attack, the oscillation amplitude and the reduced frequency.

The directions of hysteresis loops at x/c=5, 10% for the upper surface are clockwise which indicate the motion has lead phase, (figures 5a, b). This indicates that the flow in increasing the equivalent angle of attack leads of the decreasing equivalent angle of attack. The width of the hysteresis loops in these pressure ports at higher reduced frequency increase drastically and also the maximum pressure suction is increased for the high values. This specification is not seen for the lowest value k; because the unsteady behaviors of the flow are not significant, therefore the loop of k=0.0471 in the different positions of the airfoil is narrow. It is seen from figure 5 that the maximum pressure suction occurs at the maximum equivalent angle of attack near the leading edge (x/c=5%) about -2.9 for k=0.0942 and -2.6 for k=0.0706.

When the plunging airfoil passes the static stall angle, flow reverses in the direction near the surface at the rear part of the airfoil. By increasing the equivalent angle of attack, this reversal flow progresses up to the leading edge of the airfoil; then a dynamic starting vortex forms near the leading edge. This vortex initiates near the leading edge of the airfoil, enlarges, and then moves down the airfoil [13, 15]. This starting vortex as obvious in figure 5a, for k=0.0706 happens at $\alpha_{eq}=14^\circ$ and for k=0.0942 it occurred at $\alpha_{eq}=16^\circ$. In this case, the direction of the plunging motion has been abruptly changed

in the early stages of stall vortex development. Thus the dynamic starting vortex does not have enough time to grow in the down stroke of the plunging motion (equal to the increasing equivalent angle of attack) to move away from the upper surface of the airfoil. It is observed from figures 5(a, b) that after the maximum suction a sudden undershoot of pressure coefficient diagrams happened which indicate that dynamic starting vortex begin progressed in decreasing equivalent angle of attack. The hysteresis loops cross each other at the positions 30%≤x/c≤50% and create "figure 8" shape. The direction of these two hysteresis subloops change from clockwise to counterclockwise. The sudden pressure peak in these positions is a result of the developing the leading edge vortex.

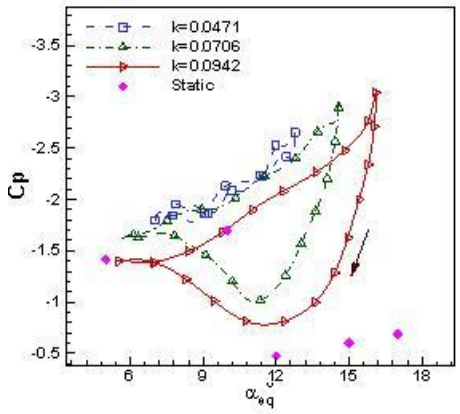

(a) x/c=5% Upper surface

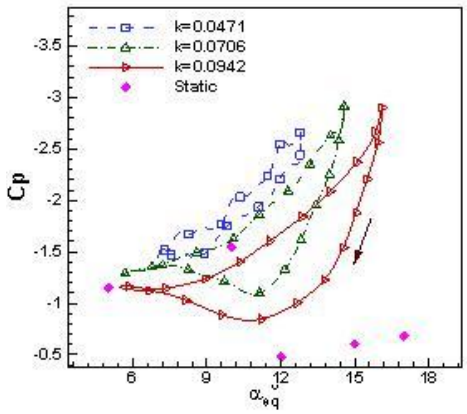

(b) x/c=10% Upper surface

Figure 5(a,b) Dynamic variation of the pressure coefficients for α_{mean}=10deg

In the position x/c=70%, the large counter clockwise loops in high equivalent angle of attack, show that the starting vortex is moved along the chord. Further, from figure 5, it is noted that at a lower reduced frequency k=0.0471, there is no indication of the sudden undershoot and progressing of the starting vortex on the airfoil. On the lower surface, figures 5(f, g), the directions of the hysteresis loops are clockwise. There is a lower pressure variations on the lower surface compared to the upper surface; which is due to the shape of the airfoil. Pressure distribution in figure 5h, on x/c=70% lower surface, is a bit different from the other ports in the lower surface. For this position, the hysteresis loops are horizontal and at k=0.0942, a small counterclockwise hysteresis loop is created. The dynamic vortex shedding to the flow induces the velocity on lower surface near the trailing edge.

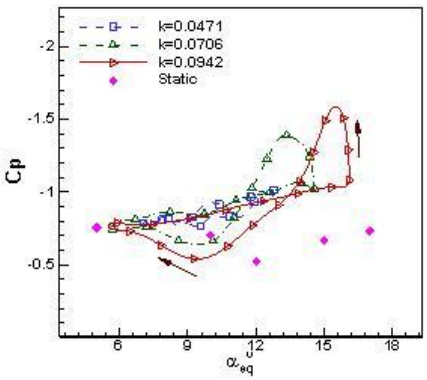

(c) x/c=30% Upper surface

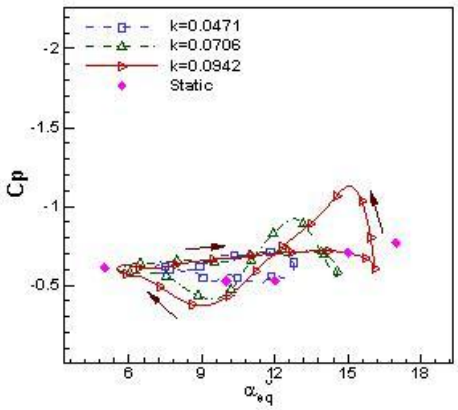

(d) x/c=50% Upper surface

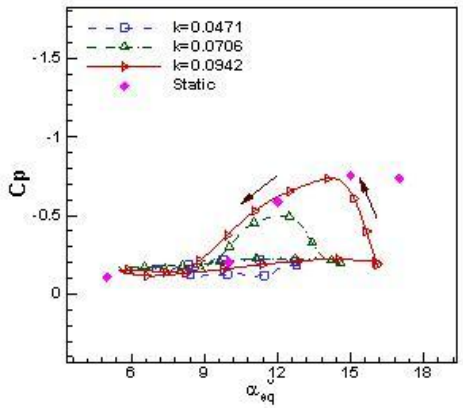

(e) x/c=70% Upper surface

Figure 5(c,d,e) Dynamic variation of the pressure coefficients for α_{mean}=10deg

Figures 6 (a, b) illustrate the variations of pressure coefficient against nondimensional time in one cycle of oscillations for several positions in upper and lower surface of the airfoil. As obvious in these figures, because a wide range of flow separation has occurred, the variations of C_p with τ are not like cosine curve (the variations of the equivalent angle were like cosine curve).

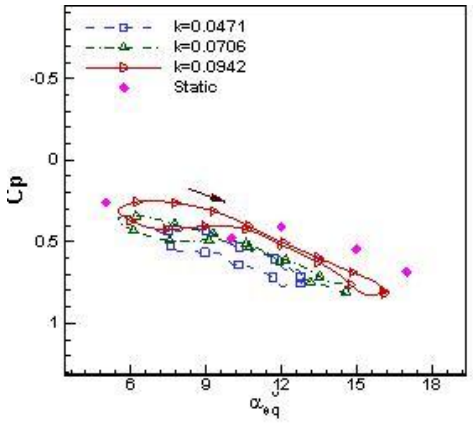

(f) x/c=10% Lower surface

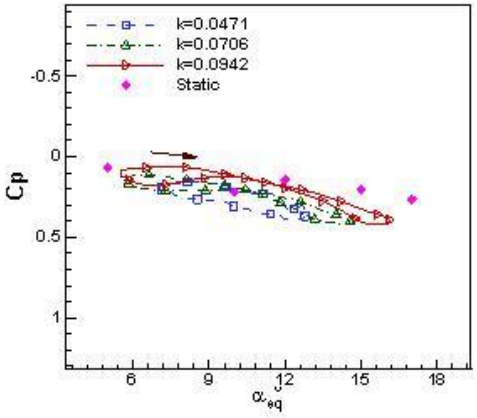

(g) x/c=30% Lower surface

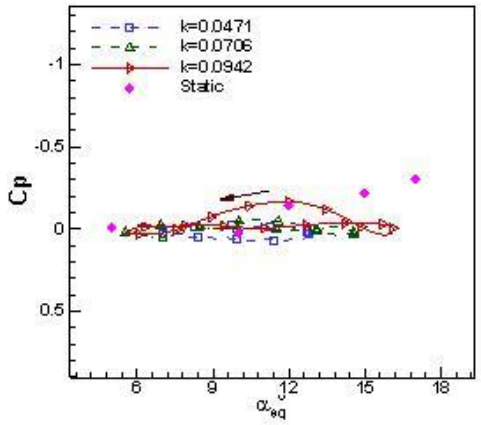

(h) x/c=70% Lower surface

Figure 5(f,g,h) Dynamic variation of the pressure coefficients for α_{mean}=10deg

As mentioned above at α_{mean}=10deg, the dynamic starting vortex is formed near the leading edge of the airfoil. The variation ranges of equivalent angle for k= 0.0706 is from 5.6 to 14.3 deg. (illustrated in figure 5), which pass the static stall angle, but this range is not wide enough for the deep dynamic stall to be happened; consequently, the starting vortex moves downward in the decreasing equivalent angle (instead of increasing). In figure 6(a), a suction peak in the instantaneous pressure distribution has been observed to remain approximately coincident with the chord wise location of the vortex. The C_p variation on the lower surface near the leading edge is higher than that of the trailing edge, (figure 6(b)).

When the time varies between 0.75<τ<1, the equivalent angle of attack changes from 10 to 14.32deg (down stroke motion) and then the dynamic vortex forms near the leading edge (x/c=5%) on the upper surface of the airfoil. For the times between 0-0.25, this angle varied in the range of 14.32-10 deg. Dynamic starting vortex progress along the chord up to trailing edge of the airfoil and the flow is separated in the vast area of the upper surface. As the time of oscillation changes between 0.25<τ <0.5, the equivalent angle varies from 10 to 5.68 deg.; the flow begin to attach from leading edge to trailing edge of the airfoil. At the time ranges between 0.5< τ <0.75, the equivalent angle changes between 5.68< α_{eq}<10 at which the airfoil is in upstroke motion, the C_p absolute value begins to increase near the leading edge ports of the airfoil. So it can be concluded that the maximum equivalent angle of attack happens when the airfoil passes in the middle of oscillations during down stroke plunging motion. A carpet diagram in figure 7 provides a good understating of the starting dynamic vortex at higher equivalent angles of attack and growing of this vortex in low equivalent angles. This picture indicates that the vortex initiation occurs in the range 0.95<τ<1 and growth and shedding of this vortex happens in 0<τ<0.25. Figure 8 depicts the aerodynamic loads of the plunging airfoil near the static stall angle for k=0.0706 and 0.0942. The C_l diagram for each reduced frequency plots the loops divided into two subloops, one of them is wider and bigger and traces counterclockwise curves and the other one is small and clockwise. A sudden overshoot in the small hysteresis loop in each reduced frequency diagram during increasing equivalent angle (downstroke motion) is the result of starting dynamic vortex creation (shown in figure 8 a); and the undershoot of the C_l diagram is due to the developing the leading edge vortex in (upstroke motion) decreasing equivalent angles. It is noticeable that stall onset is postponed well above the static stall angle.

The energy transfer between an oscillating airfoil and the surrounding airstream are discussed by a damping coefficient, $C_w = \oint C_m d\alpha$. Positive damping implies an energy transfer from the airfoil to the airstream and negative damping implies that the airfoil receives energy from the air, causing the amplitude of the motion to increase with time [16, 17]. It has been shown in figure 8 b the pitching moment diagram that two sub hysteresis loops are developed so that the moment curves look like figure 8. In each reduced frequency, a second clockwise loop provides a negative damping. The first loop is counterclockwise and decreases the amplitude of oscillation. A vortex formation near the leading edge creates the large nose-down pitching moment at high equivalent angles. The flow then

reattaches when the equivalent angle of attack is low enough and reverts to the attached flow behaviors. The slope of the pitching moment coefficient during the decrease of the equivalent angle i.e. for k=0.0942, is positive up to α_{eq}=9.5 deg. This indicates that the center of pressure moves toward the leading edge. The size of sub hystresis loops for both C_l and C_m diagrams are increased as the reduced frequency increases and the crossover points of subloops are formed in higher equivalent angle of attack. Increasing the reduced frequency acts to delay the onset of stall (moment break) to a higher angle of attack, i.e. in k=0.0706 the onset of dynamic stall is at α_{eq}=14 deg. but for k=0.0942 it happens at α_{eq}=16 deg.

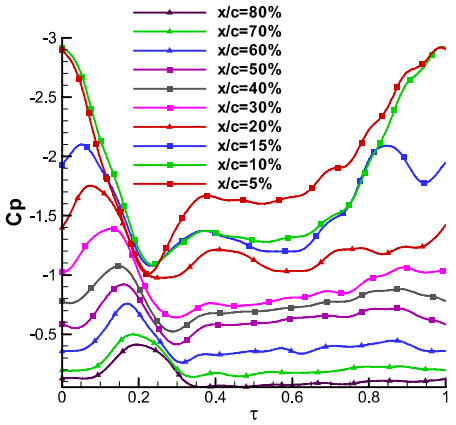

(a) Upper surface Ports

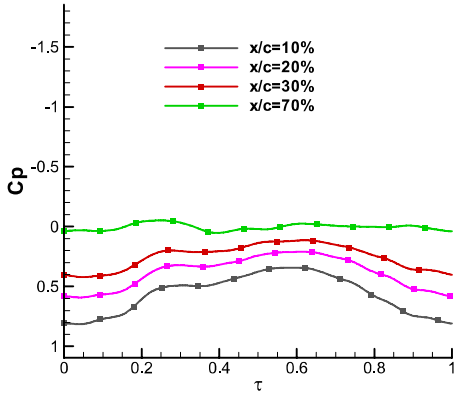

(b) Lower surface Ports

Figure 6 Variations of C_p with time (α_{mean}=10deg, k=0.0706)

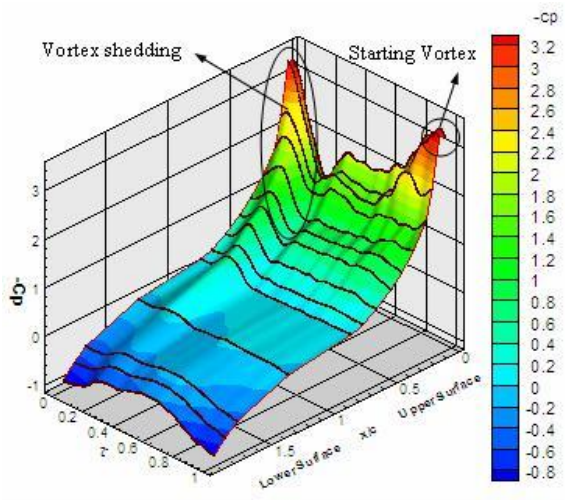

Figure 7 pressure distributions of onset stall (α_{mean}=10deg, k=0.0706)

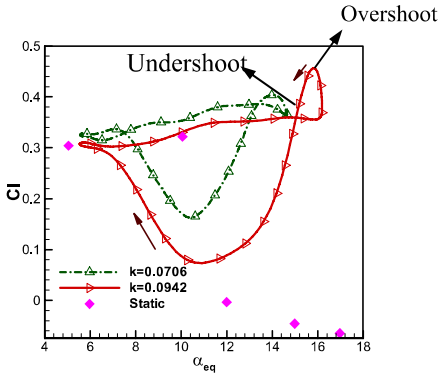

Figure 8a Variations of C_l with equivalent angle of attack (α_{mean}=10deg)

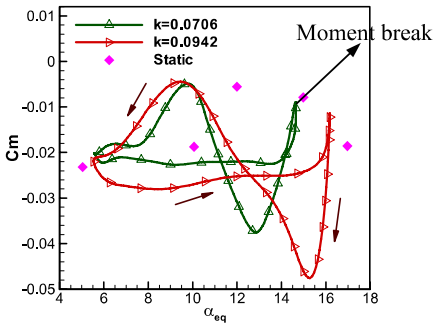

Figure 8b Variations of C_m with equivalent angle of attack (α_{mean}=10deg)

CONCLUSION

An extensive experimental study was conducted to investigate the flow phenomena over the plunging airfoil. Static pressure distributions at 14 positions over and under the model were measured. The details of the aerodynamic loads behaviors are investigated above, the whole observations summarized as follows:

- The differences in the aerodynamic loads for the upstroke and down stroke motions created hysteresis loops in unsteady motion.
- The directions of C_p hysteresis loops at x/c=5, 10% for the upper surface were clockwise (lead phase).
- The C_p hysteresis loops cross each other at the positions 30%≤x/c≤50% and create "figure 8" shape.
- The maximum pressure suction was happened near the leading edge at the highest equivalent angle of attack.
- When the equivalent angle of attack passed static stall angle, dynamic starting vortex formed near the leading edge.
- The starting vortex created in increasing equivalent angle and developing of this vortex occurred in decreasing angle.
- The variation of the C_p vs. time in stall onset was not like cosine curve.
- At the aft portions of the airfoil, the dynamic variations of the pressure coefficient were lower relative to the forward portion.
- The size of hysteresis loops of the lift coefficient were increased with higher reduced frequency.
- The pitching moment diagram was look like figure eight shape; the second clockwise loop provided a negative damping.

REFERENCES

[1] Vladislav Klein and Keith D. Noderer, "Modeling of Aircraft Unsteady Aerodynamic Characteristics", *NASA Technical Memorandum 109120*, May 1994.

[2] Carr L. W., "Progress in Analysis and Prediction of Dynamic Stall", *Journal of Aircraft*, Vol.25, No.1, January 1988.

[3] Harris, F.D. and Pruyn, R.R., "Blade Stall-Half Fact, Half Fiction", *Journal of American Helicopter Society*, Vol. 13, No. 2, April 1968, pp. 27-48.

[4] Ham, N.D. and Garelick, M.S., "Dynamic Stall Considerations in Helicopter Rotors", *Journal of American Helicopter Society*, Vol.13, No.2, April 1968, pp. 49-55.

[5] Carta, F.O., "Experimental Investigation of the Unsteady Aerodynamic Characteristics of a NACA 0012 Airfoil", *Res.Rep. M-1283-1, United Aircraft Crop*., July 1960.

[6] McCroskey, W.J., Fisher , R.K., "Detailed Aerodynamic Measurements on a Model Rotor in the Blade Stall Regime", *Journal of American Helicopter Society*, Vol.17, No.1, Jan. 1972, pp. 20-30.

[7] Johansen, J. "Prediction of Laminar/Turbulent Transition in Airfoil flows", *Risϕ-R-987 (EN),Risϕ National Laboratory* 1977.

[8] Mani, M., Soltani M.R. and Tolouei E., "An Experimental Study of Time Lag Pressure Measurement in Different Tubes", *Amirkabir*,Vol.16, No.61-B, Spring 2005.

[9] Ajalli F., Mani M., Soltani M. "An Experimental Investigation of Pressure Distribution around a Heaving Airfoil", *The 5th International conference on Heat Transfer, Fluid Mechanics and Thermodynamics*, South Africa, Spring 2007.

[10] Carta, F. O., "A Comparison of the Pitching and Plunging Response of an Oscillating Airfoil" *NASA* CR-3172, 1979.

[11] Fukushima, T. and Dadone, L.U., "Comparison of Dynamic Stall Phenomena for Pitching and Vertical Translation Motions" *NACA* CR-2793, July 1977. [3] Harris, F.D. and Pruyn, R.R., "Blade Stall-Half Fact, Half Fiction", *Journal of American Helicopter Society*, Vol. 13, No. 2, April 1968, pp. 27-48.

[12] Lishman J.Gorden, "Principles of Helicopter Aerodynamics", *Cambridge University Press.*2000. [5] Carta, F.O., "Experimental Investigation of the Unsteady Aerodynamic Characteristics of a NACA 0012 Airfoil", *Res.Rep. M-1283-1, United Aircraft Crop*., July 1960.

[13] McAlister, K. W., Carr, L. W., "Dynamic Stall Experiments on the NACA0012 Airfoil" *NASA TP*-1100, January 1978.

[14] McCroskey, W. J., "Unsteady Airfoils", *Annual Report of Fluid Mechanics*, Vol. 14, pp.285-311, 1982.

[15] Lishman , J., "Challenges in Modeling the Unsteady Aerodynamics of Wind Turbine" *AIAA 2002-0037, 21st ASME Wind Energy Symposium and 40th AIAA Aerospace Science Meeting*, Reno, NV, 2002.

[16] M.S. Francis and J.E. Keesee, "Airfoil Dynamic Stall Performance with Large Amplitude Motions," *AIAA Journal*, Vol.23, No.11, 1985, PP. 1653-1659.

[17] Joppe Johansen, "Unsteady Airfoil Flows with Application to Aeroelastic Stability," *Risϕ National Laboratory, Roskilde*, Denmark, 1999.